SSRG International Journal of Electronics and Communication Engineering
ISSN: 2348-8549/ https://doi.org/10.14445/23488549/IJECE-V11I10P106

Volume 11 Issue 10, 77-90, October 2024

Original Article

Simulation and Innovative Digital Modeling Approach for Improving the Dynamic Performances of HVDC-MMC Systems: Case of an AVM-MMC Migration

AbdeL–Hamid Mahamat Ali[1], Luc Vivien Assiene Mouodo[2], Nna Nna Theodore Patrice[3], Jean Gaston TAMBA[3], Petros Axaopoulos[4]

[1]*Engineering Electrical, National Higher Institute University, Ndjamena, Chad.*
[2]*Engineering Electrical, Higher Normal School of Technical Education University, Douala, Cameroon.*
[3]*Engineering Electrical, Institute of Technology University, Douala, Cameroun.*
[4]*Mechanical Engineering, University of West Attica, Aegaleo, Greece.*

[2]*Corresponding Author : assienemouodolucvivien@yahoo.fr*

Received: 06 August 2024 Revised: 07 September 2024 Accepted: 06 October 2024 Published: 30 October 2024

Abstract *- This article proposes innovative digital modeling by improving the control, especially the complexity of HVDC-MMC systems, by considerably limiting the high calculation load for sub-modules grouping power electronics switches during high voltage transit. In this approach, the methodology consists of directly programming the average response of the converters and their components using controlled switching sources of an average function with an addition on the harmonics and the losses of the converter, all from the current literature in and associated with the Matlab software Simulink 2022.b. secondly, a cross comparison is carried out between a real MMC architecture and a reconfigured AVM-MMC model by highlighting the value of the THD at the output. The results obtained with the AVM-MMC architecture are obtained in Simulation on a Microsoft Windows 10 operating system with an Intel Corei7-6700HQ processor at 2.60 GHz and 32 GB of RAM, with Matlab Simulink 2022.b. a simulation window of 10µs and a system operating time of 2s. Repetitive tests are carried out for 5 to 200 sub-modules, with execution time recording. We note that from 5 modules, our AVM-MMC architecture offers a direct increase of 4.6% compared to the real MMC model. This work, therefore, contributes to improving the modeling and simulation approaches of HVDC-MMC systems and the electromagnetic accounting phenomena of the power converters of their systems.*

Keywords *- HVDC system, AVM-MMC architecture, Calculation time, Comparative analysis, THD.*

1. Introduction

Electricity is traditionally produced, transported, and distributed in the form of an alternating current. It is used in this same form, except for some traction systems and industrial processes in direct current [1]. This technical choice was made during the end of the 19th century during the war of currents for major reasons, one of which is its simplicity of production (alternating generators are simpler and more reliable than direct current generators) [2], its ease of changing voltage levels using transformers, as well as its ease of interrupting the current due to the fact that it naturally cancels itself out periodically [3]. Thus, electrical networks have developed in alternating current, with large means of production deployment, connected to interconnected mesh transport networks to which the distribution networks are connected [4]. At the same time, electricity consumption needs are growing steadily and are expected to double globally. With the advent of renewable energies, the production of electrical energy is developing, which implies a need to strengthen and interconnect electrical networks [5]. It is, therefore, necessary to build very long overhead lines, underground or underwater lines, or to connect front-end networks that are sometimes asynchronous. In this area, the High Voltage Alternative Current (HVAC) transport system shows its weaknesses and limits, even its inabilities. Thanks to the evolution of power electronics, the use of high voltage direct current has become possible, giving rise to the name High Voltage Direct Current (HVDC). This technology makes it possible to transport very high powers, reaching more than 7200 MW today [6]. High voltage continuous transmission systems became very attractive for long distance power transmissions. [7]. Their principle consists of taking the alternating power supplied by one or more sources and transforming it into direct power by a converter (rectifier) [8]. The DC power then passes through a transmission line, and finally, another converter (inverter) transforms this DC power

into AC power delivered to a load or another AC network [9]. The most common is the first HVDC systems based on LCC (line commutated converter) converter technology. Their main advantage is that they can limit overcurrents when there is a fault on the DC side by controlling their phase [10]. However, they have some disadvantages that are difficult to overcome, such as:

- Control of conversion cells and optimization of their yields
- Electromagnetic compatibility phenomena of converter cells
- The strong dependence on THD delivers non-linear loads to the power converters (power switches)
- The difficulty in modeling conversion cells with several modules with a low margin of error and a simulation time in compliance with the network operating requirements of the IEEE-519-2022 standard.

1.1. Documentary Trend

Figure 1 presents the documentary evolution in terms of updated statistics available in the current literature from a combination of the keywords presented at the end of the summary. This was for four main search engines: Science Direct, Web of Science, Google Scholar, and Taylor and Francis, and it was a question of analyzing the literature on HVDC-MMC architectures, their modeling and control strategies, each time highlighting the weaknesses or the limits of his results; all on a breakdown of years from 2012-2024 for a better analysis of the new generation of HVDC-MMC systems.

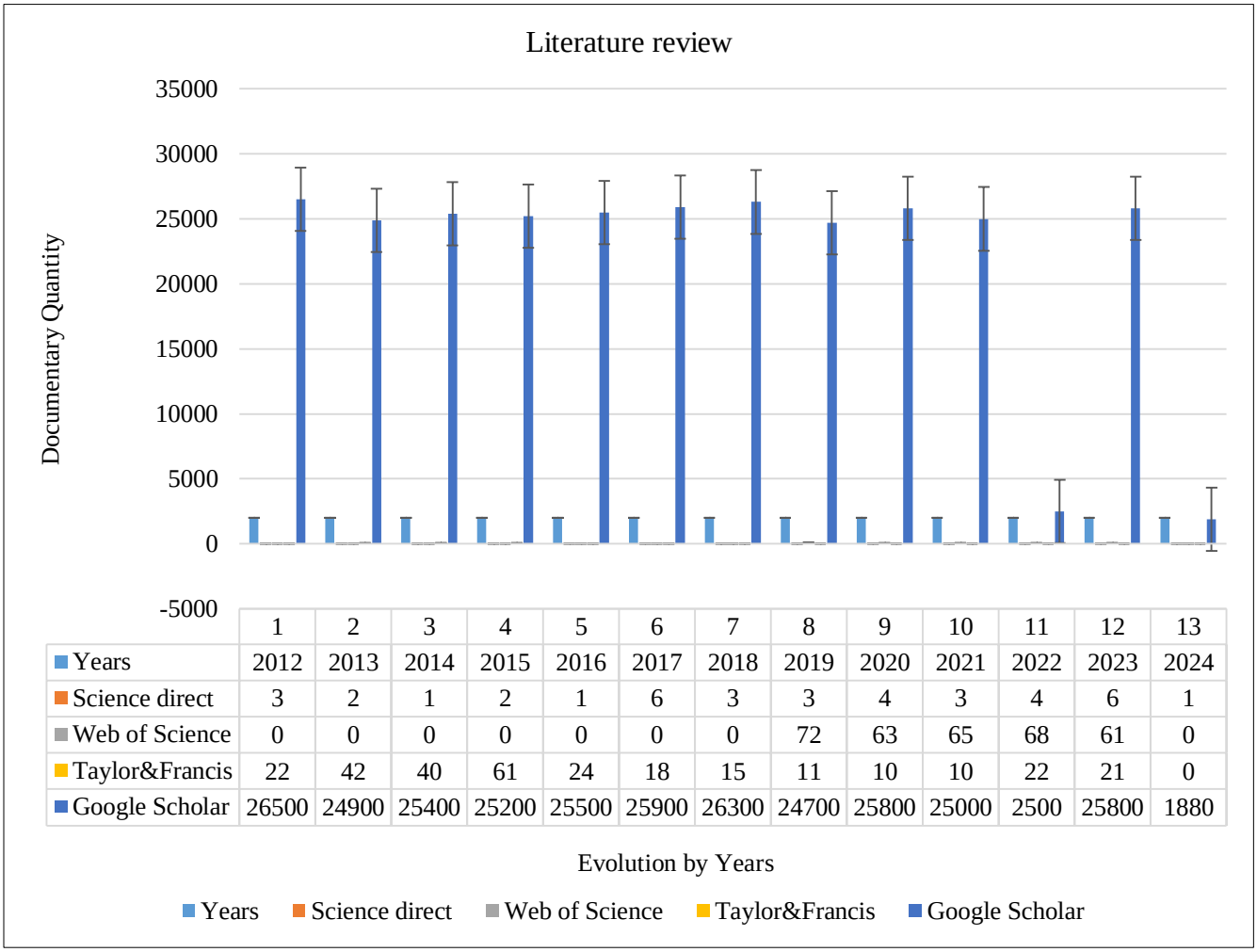

	1	2	3	4	5	6	7	8	9	10	11	12	13
Years	2012	2013	2014	2015	2016	2017	2018	2019	2020	2021	2022	2023	2024
Science direct	3	2	1	2	1	6	3	3	4	3	4	6	1
Web of Science	0	0	0	0	0	0	0	72	63	65	68	61	0
Taylor&Francis	22	42	40	61	24	18	15	11	10	10	22	21	0
Google Scholar	26500	24900	25400	25200	25500	25900	26300	24700	25800	25000	2500	25800	1880

Fig. 1 Quantity and quality documentary on HVDC-MMC systems

1.2. HVDC Based on VSC

VSC systems were extensively developed in the 1999s Hannan et al. (2018) and Oni et al. (2016) and also offered several strengths compared to conventional LCC converters Cao et al. (2013) and Song et al. (2021). Among its strong points, we can have:

• The ability to change the trajectory or direction of the flow without changing the polarity of the voltage
• Independent control of active and reactive power
• Limiting communications losses
• Less space for conversion cells

All its real benefits would be better overall modeling of HVDC systems for net production through optimization of control and forecasting.

1.3. HVDC Based on MMC

MMC modules integrated into HVDC systems also offer several advantages in their structures Lu et al. (2018) and Zhao et al. (2015). Among its advantages:

- Ease of maintenance compared to other models in the literature
- Remote control with several modulation options
- Their ability to be used and adapted in all voltage and power ranges currently handled.
- Suppression of short-circuit currents.

However, its modules must be associated with auxiliary blocks to limit conversion impurities by improving the quality of the energy. On the other hand, the greater the number of modules, the more resonance and compatibility phenomena will be present.

1.4. Paper Contributions

This article simultaneously offers several solutions when the number of converter modules increases with the voltage level. Therefore, it becomes very difficult to predict the overall behavior of the HVDC system with many non-linear components, thereby increasing the online THD levels.

On the other hand, the computing power necessary for real-time control of IGBT power switches, for example, limits the capabilities of supervision systems. The major contributions of this article are:

- Innovative digital modeling is achieved by improving the control and, especially, the complexity of HVDC-MMC systems when the number of modules is large at the level of the converter cells.
- A direct limitation of the resonance phenomenon is due to non-linear loads in the converters, which result in a considerable reduction in THD.

Table 1. Evolution of the challenges of HVDC systems

Developments Over the Years	Some Achievements or Advances in the Field
1800	Construction of the first electric battery by Alessandro VOLTA. To obtain a direct current, he stacks copper and zinc disks alternately. Each pair is separated from its neighbor by a cloth soaked in salt water. From this assembly, it obtains direct current [3]. Following these experiments, Thomas Edison built the first electrical power system, including a generator, cables, and loads [4].
1882	Operation of Pearl Street Station in New York. It was a continuous system (DC: Direct Current) in which the generator provided power to 59 consumers arranged within an approximately 1.5 km radius [4].
1889	The first single-phase AC transmission line between Willamette Falls and Portland operates in Oregon. The development of polyphase systems by Nikola TESLA then marked the emergence of AC systems, so much so that they emerged victorious in the battle against DC systems [4].
1950	The development of mercury switches in HVDC high voltage direct current transmission systems has become attractive for long-distance transmissions [4].
1954	The first power transmission using HVDC systems was commercialized. This was an interconnection between the island of Gotland and mainland Sweden. It was carried out via a 96 km long submarine cable, ensuring power transmission of 20 MW with a nominal voltage of 100 kV [4]
1972	The first connection used only thyristors: the Eel River project made it possible to connect Quebec and New Brunswick, which are two asynchronous zones. This back-to-back type connection used four thyristors in parallel per arm to be able to carry enough current. These thyristors are less expensive than mercury vapor diodes and minimize operating costs [9].
1985	Considerable improvement in thyristors: water-cooled and air-insulated thyristors can withstand higher currents and voltages. This reduces the need to put thyristors in parallel or series or to call on different auxiliary services [9].
1986	First VSC type link: It offers new advantages, including independent control of reactive and active powers and the supply of a weak network without power generation [9].
2010	First MMC type link: This new topology makes it possible to reduce losses and the need for filters. Today, most HVDC link manufacturers offer VSC solutions based on MMC technology. The Trans Bay Cable link makes it possible to transmit 400 MW with a DC bus ± 200 KV and converters comprising 216 sub-modules per arm [9].
2019	Commissioning of the joint venture project between British National Grid (Richborough) and Belgian Elia (Zeebrugge) [7] using an HVDC submarine power cable named Nemo Link. This interconnection transmits 1000 MW at 400 KV over 140 km, including 130 km underwater and the rest buried in the ground 60 m deep.

- Limitation of auxiliary blocks for energy quality with filters at the converter output.
- Compared to the current literature, there is a considerable reduction in the computing power necessary to control the switches of the sub-modules.
- Statistical validation based on certain indicators with Principal Component Analysis (PCA)

All his contributions will be developed in this article in several sections; thus, in Section 2, a chronological issue of HVDC systems according to the literature will be presented; in Section 3, in-depth mathematical modeling of the different architectures will be revealed with hypotheses allowing simplified numerical modeling to be carried out with clearly defined values for the simulation. Section 4 reveals the simulation results, and a comparison with the literature is made with statistical validation. Section 5 contains a conclusion reminding the main contributions or originalities and perspectives.

1.4.1. State of Evolution of the Issues of HVDC Systems in the Literature

Table 1 presents the major ones in which HVDC architectures have been developed. Nowadays, the stakes are even more important. This is why several researchers are interested in modeling, especially in the optimal supervision of the operations of HVDC lines in normal or disturbed operations.

2. Modeling of an HVDC –MMC Connection

The MMC converter is a very advanced technique based on the HVDC link. This new arrangement has the advantage of reducing the switching frequency, thus causing certain losses. With switches for each switching level, this switching position can be seen in Figure 2

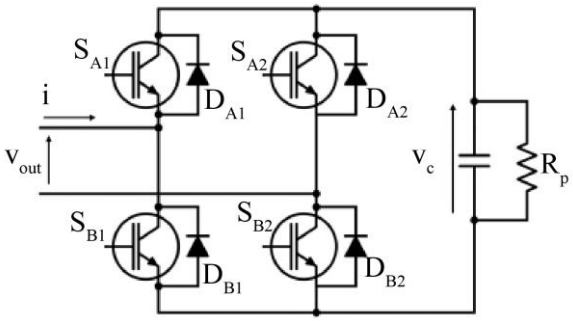

Fig. 2 Full bridge module of an MMC converter for one arm

This configuration can have an equivalence from an average value, thus offering modeling simplicity, as presented in Figure 3. Therefore, this simplification is implemented in the overall architecture of Figure 4 for a point-to-structure-point MMC-HVDC system. Figure 5 provides a detailed topology of the MMC architecture for several sub-modules.

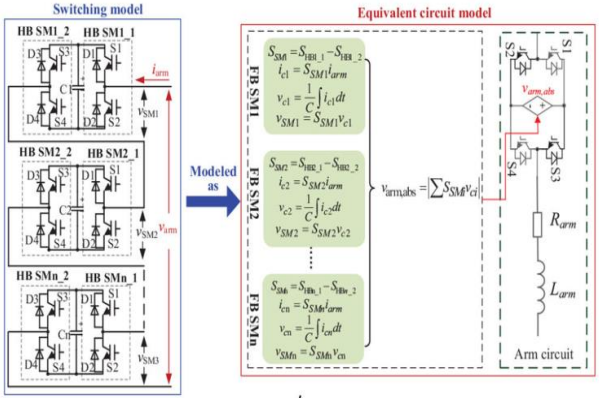

Fig. 3 Equivalent circuit of the MMC model

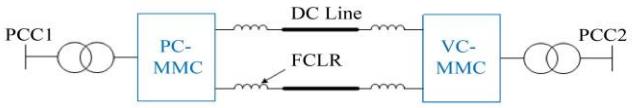

Fig. 4 MMC-HVDC point-to-point system structure

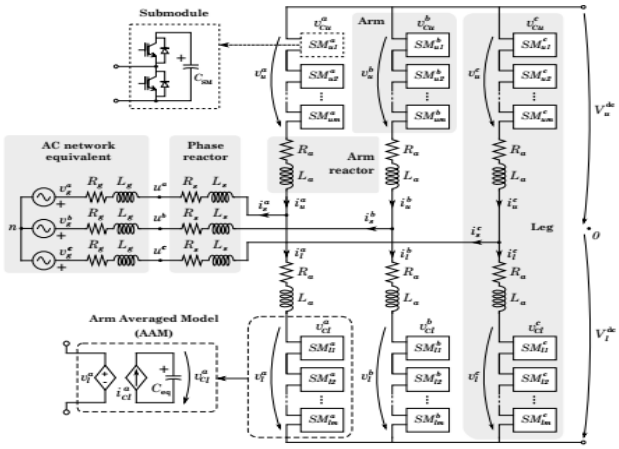

Fig. 5 Detailed MMC topology

This architecture in Figure 5, which represents the third generation of HVDC systems, already offers several advantages. Our ambition in this article is to optimize these advantages by an AVM-MMC architectural reconfiguration with innovative digital modeling by improving the control, especially the complexity, which limits the calculation load for the command and control of power switches and indicators performance such as THD. Therefore, this research aims to highlight all the advantages of the AVM-MMC architecture compared to the real MMC model, which has some limitations.

2.1. MMC System Using the AVM Approach

In this section, the methodological approach consists of using the simplified mathematical models of Figure 7 in the Simulink Matlab environment with the main objectives of limiting the computing power and especially the nonlinearity of the power electronics components, all according to specific

constraints. By considering only the low frequency components of the currents and voltages, that is to say, by neglecting the switching frequency components produced by the converter, it is possible to draw the equivalent circuit presented in Figure 6.

As study hypotheses:

• All SMs have identical capacitors, and the voltages across them are equal and balanced;

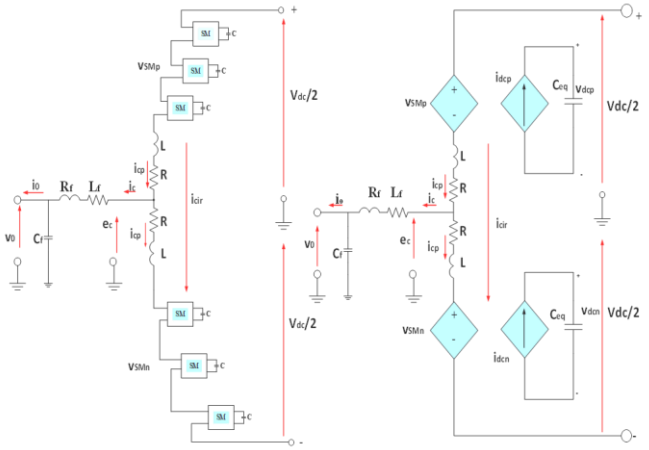

(a) **(b)**

Fig. 6(a) An arm of the MMC topology, and (b) AVM of the arm of a MMC .

The switching frequency and the number of SMs per arm are infinite; $\frac{v_{dc}}{2}$ is ideal, the resistances and inductances on the half-arms are identical.

With the law of knots:

$i_c = i_p - i_n$; $i_{cir} = \frac{i_p + i_n}{2}$ (circulating current). The variables are related to the average value over a switching cycle. The blocks in each arm are replaced by a pair of controlled sources representing both the AC side voltage and the DC side current of the SMs. The MMC equivalent capacitance Ceq includes the equivalent series representation of DC rated capacitors. The capacity Ceq corresponds to C/N, with N the number of SMs connected per leg. This can be observed in Figure 7.

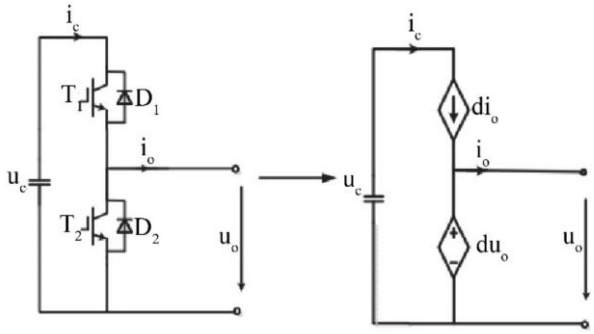

Fig. 7 Half-bridge circuit and its average value model

2.2. Mathematical Equations of the Mean Value Model

With k chosen as the phase index, the SMs of each arm of the converter are described as follows:

$$v_{SM}^{kp} = m_p^k v_{dc}^{kp} \qquad v_{SM}^{kn} = m_n^k v_{dc}^{kn} \tag{1}$$

$$i_{dc}^{KP} = m_p^k i_{cp}^k$$
$$i_{dc}^{Kn} = m_n^k i_{cn}^k$$

The tensions v_{SM}^{kp} and v_{SM}^{kn} represent the equivalent AC voltages produced by the upper and lower arms of the SMs respectively. The currents i_{dc}^{KP} and i_{dc}^{Kn} are equivalent currents on the side CC. The average current flows through the DC side capacitors over a switching period. The tensions v_{dc}^{kp} are equivalent to average voltages on the direct current side (over a switching period) and are insertion indices calculated to control the alternating voltage produced and attenuating unwanted components of the circulating current. Following Figure 6(b), we can deduce from the two half-arms, according to Kirchhoff's theorem, the following relationships:

$$\begin{cases} L\frac{di_{cp}^k}{dt} = -e_c^k + \frac{v_{dc}}{2} - m_p^k v_{dc}^{kp} - Ri_{cp}^k \\ L\frac{di_{cp}^k}{dt} = e_c^k + \frac{v_{dc}}{2} - m_n^k v_{dc}^{kn} - Ri_{cp}^k \end{cases} \tag{2}$$

So, leaving e_{cir}^k be the second order harmonic component of e_{RL}^{kp} and e_{RL}^{kn} the calculation of the insertion indices of the upper and lower arms can be done by (3) [13].

$$\begin{cases} m_p^k = \frac{1 - e_c^k - e_{cir}^k}{2} \\ m_n^k = \frac{1 + e_c^k - e_{cir}^k}{2} \end{cases} \tag{3}$$

Based on this average model, corresponding equations were posed for fewer variables. Line currents i_c^k and circulation currents i_{cir}^k are preferred as state variables. Thus, the upper arm currents i_{cp}^k and lower arm i_{cn}^k can be represented as follows [14, 15, 16, 17]:

$$\begin{cases} i_{cp}^k = i_{cir}^k + \frac{1}{2} i_c^k \\ i_{cn}^k = i_{cir}^k - \frac{1}{2} i_c^k \end{cases} \tag{4}$$

Considering Equations (3) and (4) and the equivalent DC voltages of each half-arm, the average value model of an arm of an MMC is given by Equation (5).

$$\frac{d}{dt}\begin{bmatrix} i_{cir} \\ v_p^{\Sigma} \\ v_n^{\Sigma} \end{bmatrix} = \begin{bmatrix} -\frac{R}{L} & \frac{-m_p}{2} & \frac{-m_n}{2} \\ \frac{m_p}{Ceq_{arm}} & 0 & 0 \\ \frac{m_n}{Ceq_{arm}} & 0 & 0 \end{bmatrix} \begin{bmatrix} i_{cir} \\ v_p^{\Sigma} \\ v_n^{\Sigma} \end{bmatrix} + \begin{bmatrix} \frac{V_{dc}}{2} \\ \frac{m_p i_c}{2Ceq_{arm}} \\ -\frac{m_n i_c}{2Ceq_{arm}} \end{bmatrix} \tag{5}$$

The DC voltages of the SMs are balanced in the three arms of an MMC, so the equivalent DC voltage for each half arm can be accurately given by:

$$\begin{cases} \frac{dv_{dc}^{kp}}{dt} = \frac{m_p^k}{c_{eq}}\left(i_{cir}^k + \frac{1}{2}i_c^k\right) \\ \frac{dv_{dc}^{kn}}{dt} = \frac{m_n^k}{c_{eq}}\left(i_{cir}^k - \frac{1}{2}i_c^k\right) \end{cases} \quad (6)$$

By imposing the circulation current in each half-arm, depending on the mesh, the system (6) becomes:

$$\begin{cases} L\left(\frac{di_{cir}^k}{dt} + \frac{1}{2}\frac{di_c^k}{dt}\right) = -e_c^k - R\left(i_{cir}^k + \frac{1}{2}i_c^k\right) - v_{SM}^{kp} + \frac{v_{dc}}{2} \\ L\left(\frac{di_{cir}^k}{dt} + \frac{1}{2}\frac{di_c^k}{dt}\right) = e_c^k - R\left(i_{cir}^k - \frac{1}{2}i_c^k\right) - v_{SM}^{kn} + \frac{v_{dc}}{2} \end{cases} \quad (7)$$

Concerning the output path of the converter, it is also possible to arrive at the following result:

$$e_c^k - R_f i_c^k - L_f \frac{di_c^k}{dt} = v_0^k \quad (8)$$

v_0^k Represents the phase-neutral voltages supplied to the load by the MMC. The dynamic current circulation Equation obtained from (7) is:

$$\frac{di_{cir}^k}{dt} = -\frac{R}{L}i_{cir}^k - \frac{1}{2L}v_{SM}^{kp} - \frac{1}{2L}v_{SM}^{kn} + \frac{1}{2L}v_{dc} \quad (9)$$

The differential equation for line current can be obtained by combining the addition of (7) and (8).

$$\frac{di_{cir}^k}{dt} = \frac{1}{L+2L_f}\left(v_{SM}^{kn} - v_{SM}^{kp}\right) - \frac{1}{L+2L_f}v_0^k - \frac{R+2R_f}{L+2L_f}i_c^k \quad (10)$$

Equations (6), (9), and (10) form a state space model of the MMC presented in (11).

$$\begin{cases} \frac{dv_{dc}^{kp}}{dt} = \frac{m_p^k}{c_{eq}}\left(i_{cir}^k + \frac{1}{2}i_c^k\right) \\ \frac{dv_{dc}^{kn}}{dt} = \frac{m_n^k}{c_{eq}}\left(i_{cir}^k - \frac{1}{2}i_c^k\right) \\ \frac{di_{cir}^k}{dt} = -\frac{R}{L}i_{cir}^k - \frac{1}{2L}v_{SM}^{kp} - \frac{1}{2L}v_{SM}^{kn} + \frac{1}{2L}v_{dc} \\ \frac{di_c^k}{dt} = \frac{1}{L+2L_f}\left(v_{SM}^{kn} - v_{SM}^{kp}\right) - \frac{2}{L+2L_f}v_0^k - \frac{R+2R_f}{L+2L_f}i_c^k \end{cases} \quad (11)$$

To simplify mathematical processing, two new state variables v_{dc}^{Δ} and v_{dc}^{Σ} are introduced [18-21]:

$$v_{dc}^{\Delta} = v_{dc}^{kp} + v_{dc}^{kn} \quad (12)$$

$$v_{dc}^{\Sigma} = v_{dc}^{kp} - v_{dc}^{kn} \quad (13)$$

The state space model can be rewritten as follows, and we obtain nonlinear differential equations:

$$2C_{eq}\frac{dv_{dc}^{k\Sigma}}{dt} = 2(1 - e_{cir}^{k*})i_{cir}^k - e_c^{k*}i_c^k \quad (14)$$

$$2C_{eq}\frac{dv_{dc}^{k\Delta}}{dt} = -2e_c^{k*}i_{cir}^k + (1 - e_{cir}^{k*})i_c^k \quad (15)$$

$$4L\frac{di_{cir}^k}{dt} = -4Ri_{cir}^k - (1 - e_{cir}^{k*})v_{dc}^{k\Sigma} + e_c^{k*}v_{dc}^{\Delta} + 2v_{dc} \quad (16)$$

$$2(L + 2L_f)\frac{di_c^k}{dt} = e_c^{k*}v_{dc}^{k\Sigma} - (1 - e_{cir}^{k*})v_{dc}^{k\Delta} - 4v_0^k - 2(R + 2R_f)i_c^k \quad (17)$$

By linearizing (14) and (15), we obtain:

$$2\mathrm{C_{eq}}\frac{\mathrm{d}\tilde{\mathrm{v}}_{\mathrm{dc}}^{\mathrm{k}\Sigma}}{\mathrm{dt}} = 2(1 - \mathrm{e_{cir0}^{k*}})\tilde{\mathrm{i}}_{\mathrm{cir}}^{\mathrm{k}} - 2\mathrm{i_{cir0}^{k}}\tilde{\mathrm{e}}_{\mathrm{cir}}^{\mathrm{k*}} - \mathrm{i_{co}^{k*}}\tilde{\mathrm{i}}_{\mathrm{c}}^{\mathrm{k}} - \mathrm{i_{co}^{k}}\tilde{\mathrm{e}}_{\mathrm{c}}^{\mathrm{k*}} \quad (18)$$

By transforming Equation (18) in the Laplace domain, the equation becomes:

$$2(\mathrm{Z} + 2\mathrm{Z_f})\tilde{\mathrm{I}}_{\mathrm{c}}^{\mathrm{k}}(\mathrm{s}) = 2\mathrm{V_{dc0}}\tilde{\mathrm{E}}_{\mathrm{c}}^{\mathrm{k*}}(\mathrm{s}) - 4\tilde{\mathrm{V}}_{0}^{\mathrm{k}}(\mathrm{s}) \quad (19)$$

With: $Z = sL + R$ *and* $Z_f = sL_f + R_f$.

The following equation gives the DC side admittance equation:

$$\mathrm{Y_{dc}}(\mathrm{s}) = \frac{2\mathrm{sC_{eq}}}{4\mathrm{sC_{eq}Z}+1-\left(\frac{\mathrm{S_0}}{3\mathrm{V_{dc0}}}+2\mathrm{sC_{eq}V_{dc0}}\right)\mathrm{G_{cir}}(\mathrm{s})} \quad (20)$$

With: G_{cir} circulating current controller.

The equation for the current control loop is:

$$\tilde{I}_c^k(s) = G_i^{cl}(s)\, I_c^{k*}(s) - Y_{ac}(s)\tilde{V}_0^k(s) \quad (21)$$

$$\text{With } G_i^{cl}(s) = \frac{\left(4\mathrm{sC_{eq}V_{dc0}}+\frac{2\mathrm{S_0}}{3\mathrm{V_{dc0}}}\right)}{4\mathrm{sC_{eq}\,(Z+2Z_f)}+(4\mathrm{sC_{eq}\,V_{dc0}}+\frac{2\mathrm{S_0}}{3\mathrm{V_{dc0}}})\mathrm{G_i(s)}+1} \quad (22)$$

$$Y_{ac}(s) = \frac{8\mathrm{sC_{eq}}}{4\mathrm{sC_{eq}\,(Z+2Z_f)}+(4\mathrm{sC_{eq}\,V_{dc0}}+\frac{2\mathrm{S_0}}{3\mathrm{V_{dc0}}})\mathrm{G_i(s)}+1} \quad (23)$$

The following relation gives the equation of the voltage control loop:

$$\tilde{V}_0^k(s) = G_v^{cl}(s)\tilde{V}_0^{k*}(s) - Z_{ac}(s)\tilde{I}_c^k(s) \quad (24)$$

$$\text{With } G_v^{cl}(s) = \frac{G_i^{cl}(s)G_v(s)}{Y_{ac}(s)+G_i^{cl}(s)G_v(s)} \quad (25)$$

$$Z_{ac}(s) = \frac{1}{Y_{ac}(s)+G_i^{cl}(s)G_v(s)} \quad (26)$$

The equations of the Thévenin voltage in an open circuit and the equivalent Thévenin impedance in the closed loop of the system give the following expressions:

$$\tilde{V}_{th}^k = \frac{G_v^{cl}(s)\tilde{V}_0^{k*}}{sC_fZ_{ac}(s)+1} \quad (27)$$

$$Z_{th}^v = \frac{Z_{ac}(s)}{sC_fZ_{ac}(s)+1} \quad (28)$$

We, therefore, obtain the equivalent circuit of the following MMC system in Figure 8.

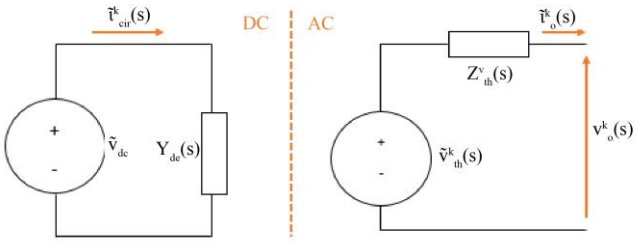

Fig. 8 Modeled MMC equivalent circuit

2.3. Control Strategy

The external control of the link is created to control the active and reactive powers injected or not by the converter into the network. While the internal control allows the MMC converter to exchange active power without the SM capacitor voltages being too affected. The PI regulator is used for external control of active and reactive power. By exploiting Equation (29), we can write in d-q the equation:

$$\begin{cases} P = \frac{3}{2}(v_d i_d + v_q i_q) \\ Q = \frac{3}{2}(v_d i_d - v_q i_q) \end{cases} \quad (29)$$

The internal control uses two PI regulators for the energy balancing and total energy control loop. The energy stored in each sub-module is equally in the half-arms and can be written [22-25]:

$$W_{cp}^{\Sigma} = \frac{C_{SM}}{2N}(V_{cp}^{\Sigma})^2 \quad (30)$$

$$W_{cn}^{\Sigma} = \frac{C_{SM}}{2N}(V_{cn}^{\Sigma})^2 \quad (31)$$

3. Results and Discussion

Table 2. Characteristics of the VSC-MMC HVDC hybrid link

Parameters from AC Source to Rectifier (VSC)			
AC Side Source Voltage	420 KV	AC Side Active Power	960 MW
Resistance Rn before the Filter	1.764 Ω	Inductance Ln before Filter C	0.56 H
Filter Capacity C	0.09 F	Transformer Y/D	420/380 KV
Resistance Rc after Filter C	1.764 Ω	Inductance Lc after Filter C	0.112 H
AC side Frequency	50 Hz	Apparent Power	1000 MVA
Continuous Bus Parameters			
Distance (Two Conductors)	400 Km	Capacity C	50µF
DC Resistance	6.9 mΩ/Km	DC Inductance	0.0795 mH/km
DC Power		Tension DC	±320 KV
AVM-MMC Inverter Parameters			
Number of Submodules	05	Inductance per Compartment	76 mH
Half Arm Resistance	0 . 8 Ω	Voltage of each SM	76 KV
Capacity of each SM	28 µF		

The objective of this section is to present the simulation advantages offered by the AVM-MMC architecture and, especially, its harmonic distortion rate, which is significantly better. The results of the AVM model simulations for circulating currents and voltages will be compared to those of the real MMC model. Then, cross-validation will be carried out using the results available in the literature. Figures 9, 10, 11 and 12 show, respectively, for the AVM-MMC model, the output voltage, the current evolution during the switching stages, and the sum of the lower and upper voltages of the different switching modules

3.1. Real Model Characteristics of MMC Inverter with PS-PWM

3.1.1. Upper and Lower Arm Tensions

Figure 13 shows the AC side voltage of the upper and lower arms of the actual MMC converter controlled by the PS-PWM. We can observe the 5 levels of the MMC at each arm with tension levels approaching the reference voltage. The voltage of 2.5 KV is close to the 320 KV reference.

Figures 14 and 15 illustrate the control (control signal) of the five-level MMC with PS-PWM and the triangular carrier of the Phase-Shifted-PWM control where we have fixed the switching frequency fc=300 Hz, which is six times the fundamental 50 Hz. The apparent switching frequency of the converter is 1500 Hz.

3.2. Discussion and Validation of Results

The results obtained with the AVM-MMC architecture are obtained in Simulation on a Microsoft Windows 10 operating system with an Intel Corei7-6700HQ processor at 2.60 GHz and 32 GB of RAM, with Matlab Simulink 2022. b for a simulation time step of 10µs and a system operating time of 2sRepetitive tests are carried out for 5 to 200 sub-modules, with execution time recording. We note that from 5 modules, our AVM-MMC architecture offers a direct comparison of 4.6% to the real MMC model. On the other hand, Tables 3, 4, and 5. Present a crossover study to validate the results of this article based on results already available in the literature.

Table 3. MMC-HVDC execution time based on SM topologies [21]

Architecture MMC in Literature	ECM Simplified Runtime (s)	Authors	Years
HB	11.52	[21]	2019
FB	11.73	[21]	2019
CD	12.38	[21]	2019
3LX	12.21	[21]	2019
Hybrid (HB and FB)	11.94	[21]	2019

Table 4. MMC-HVDC execution time as a function of voltage levels [21]

Architecture MMC in Literature	ECM Simplified Runtime (s)	Authors	Years
20	11.73	[21]	2019
40	12.03	[21]	2019
60	12.45	[21]	2019
80	12.71	[21]	2019
100	13.12	[21]	2019
200	16.29	[21]	2019

The AVM-MMC architecture offers respective times of 2.01, 2.70, 3.40, 3.80, 4.80, 7.56. These are better than those in Tables 3 and 4, proving that the AVM-MMC architecture successfully simplifies the power of the calculations necessary to control power switches.

Figure 18 presents the convergence speed of the ECMs as a function of the number of modules and the reaction time.

Table 5. AVM-MMC execution time as a function of voltage levels

Architecture AVM- MMC	ECM Simplified Runtime (s)	Authors	Years
5	2.01	In this work	2024
20	2.70	In this work	2024
40	3.40	In this work	2024
60	3.80	In this work	2024
80	4.01	In this work	2024
100	4.80	In this work	2024
200	7.56	In this work	2024

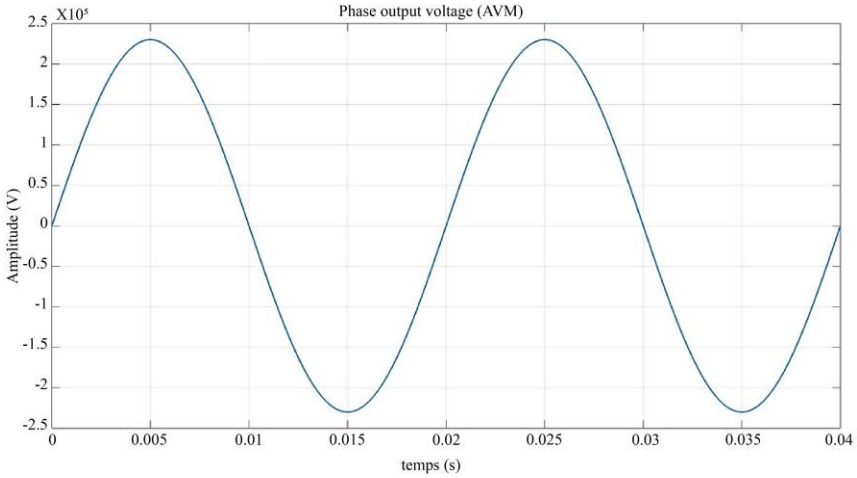

Fig. 9 AC voltage curve at the output of the AVM-MMC model

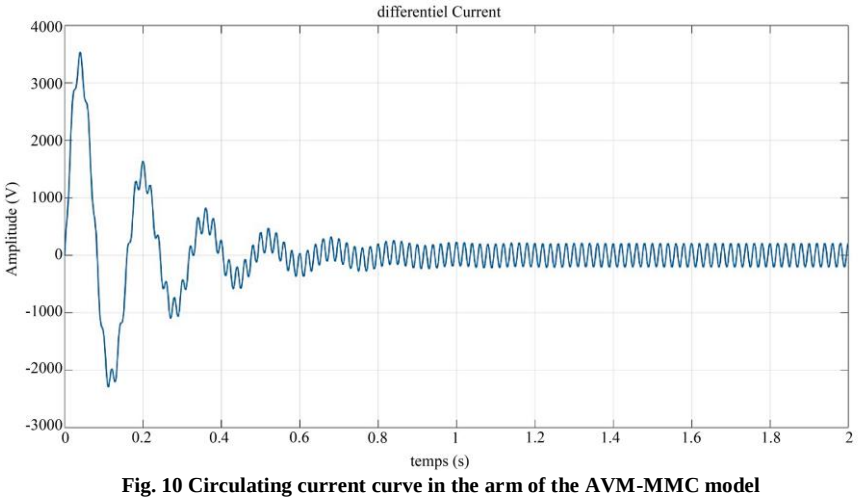

Fig. 10 Circulating current curve in the arm of the AVM-MMC model

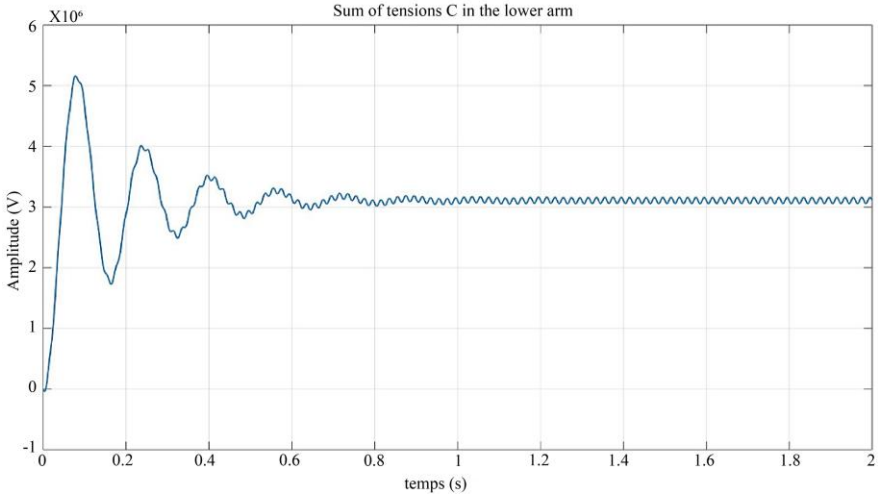

Fig. 11 Sum of the voltages of the lower arm capacities of the AVM-MMC model

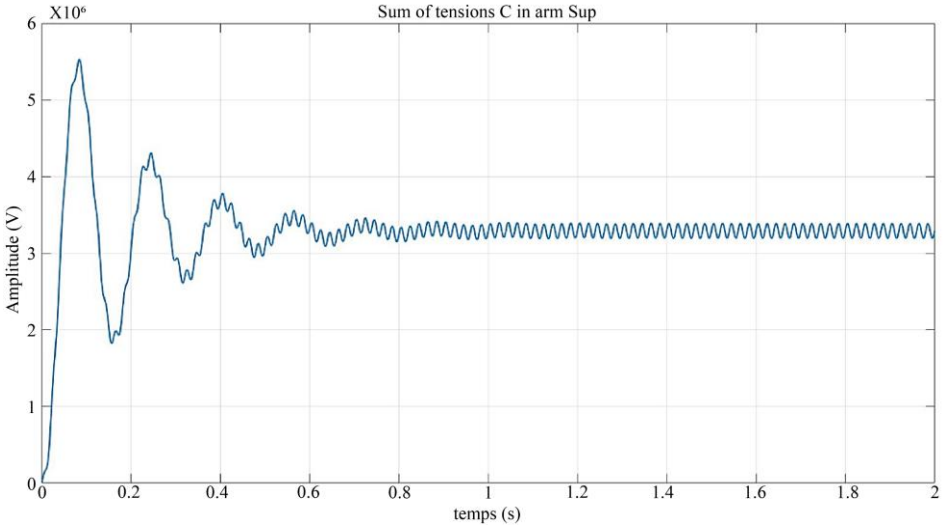

Fig. 12 Sum of the voltages of the upper arm capacities of the AVM-MMC model

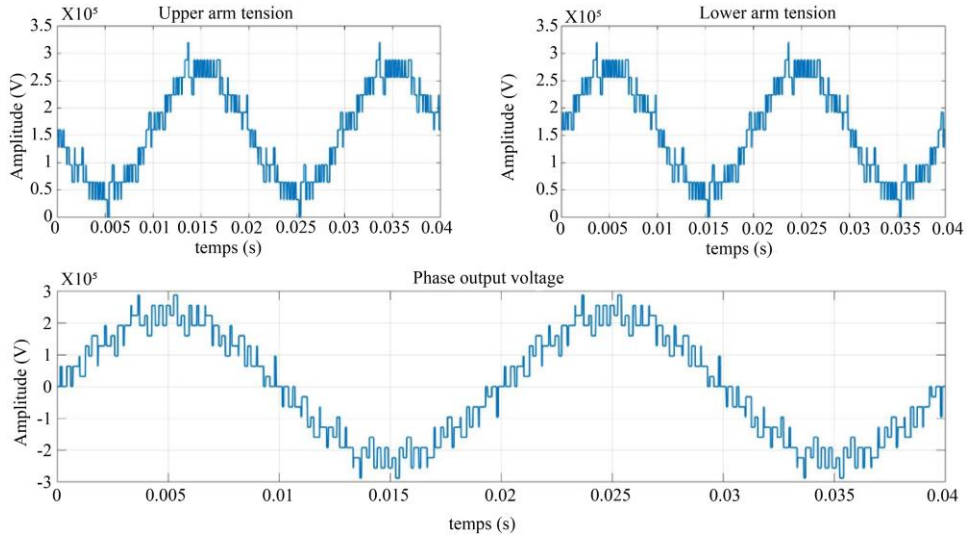

Fig. 13 Upper and lower arm tensions of the real MMC model

3.2.1. Switching Upper Arms and Lower Arms

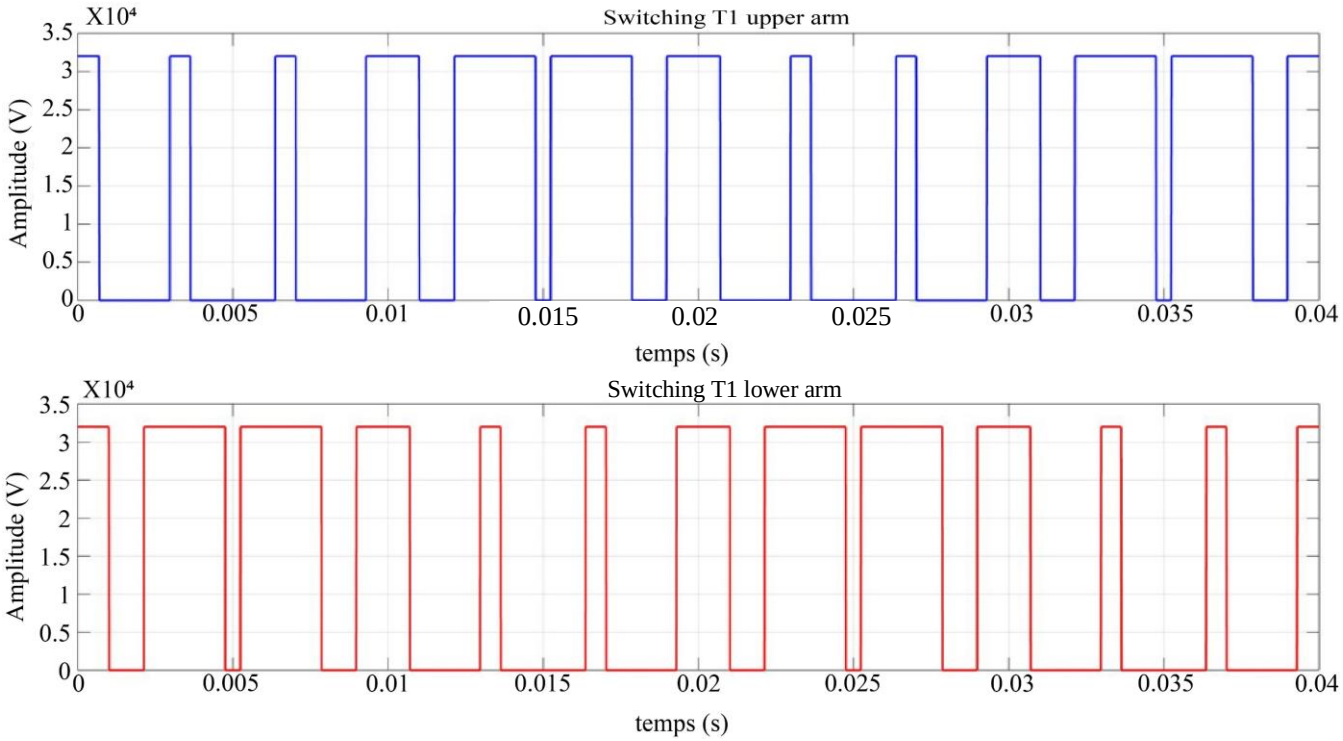

Fig. 14 Control (control signal) of the five-level MMC with PS-PWM

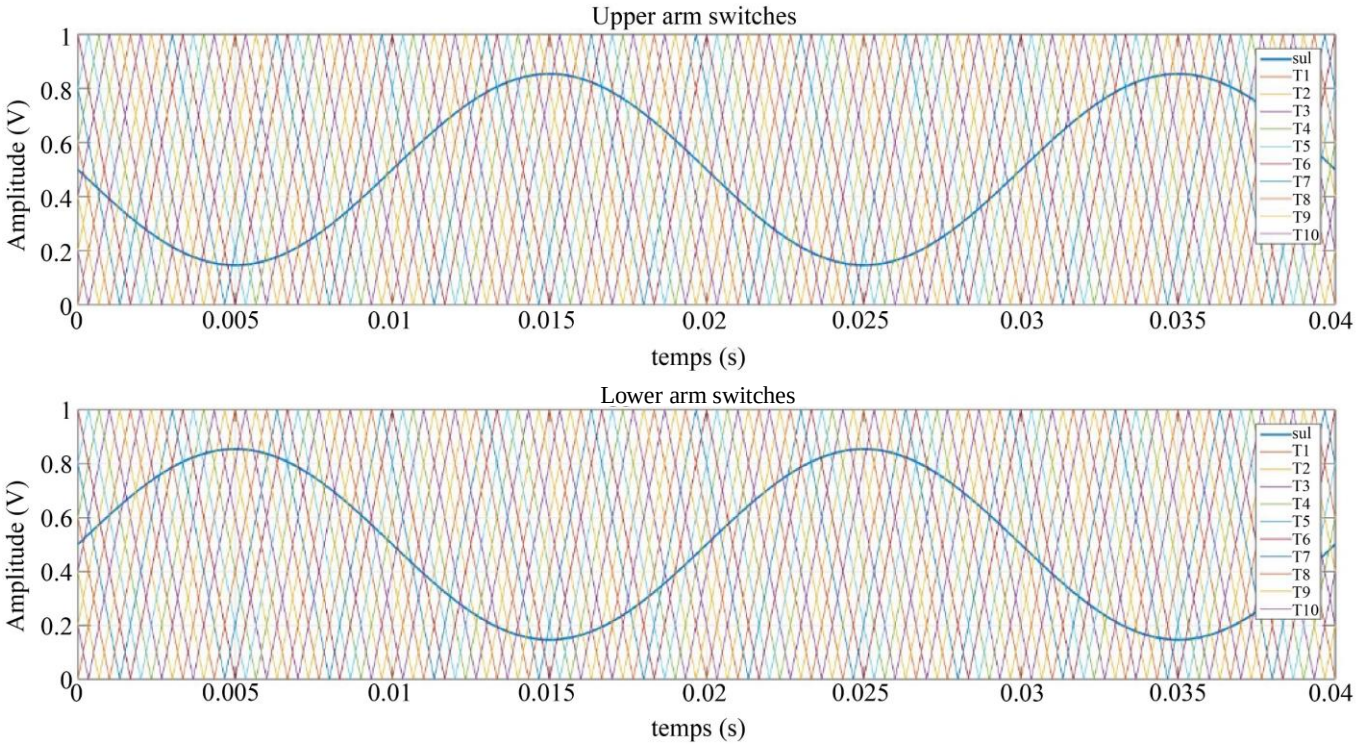

Fig. 15 Carrier and reference signal

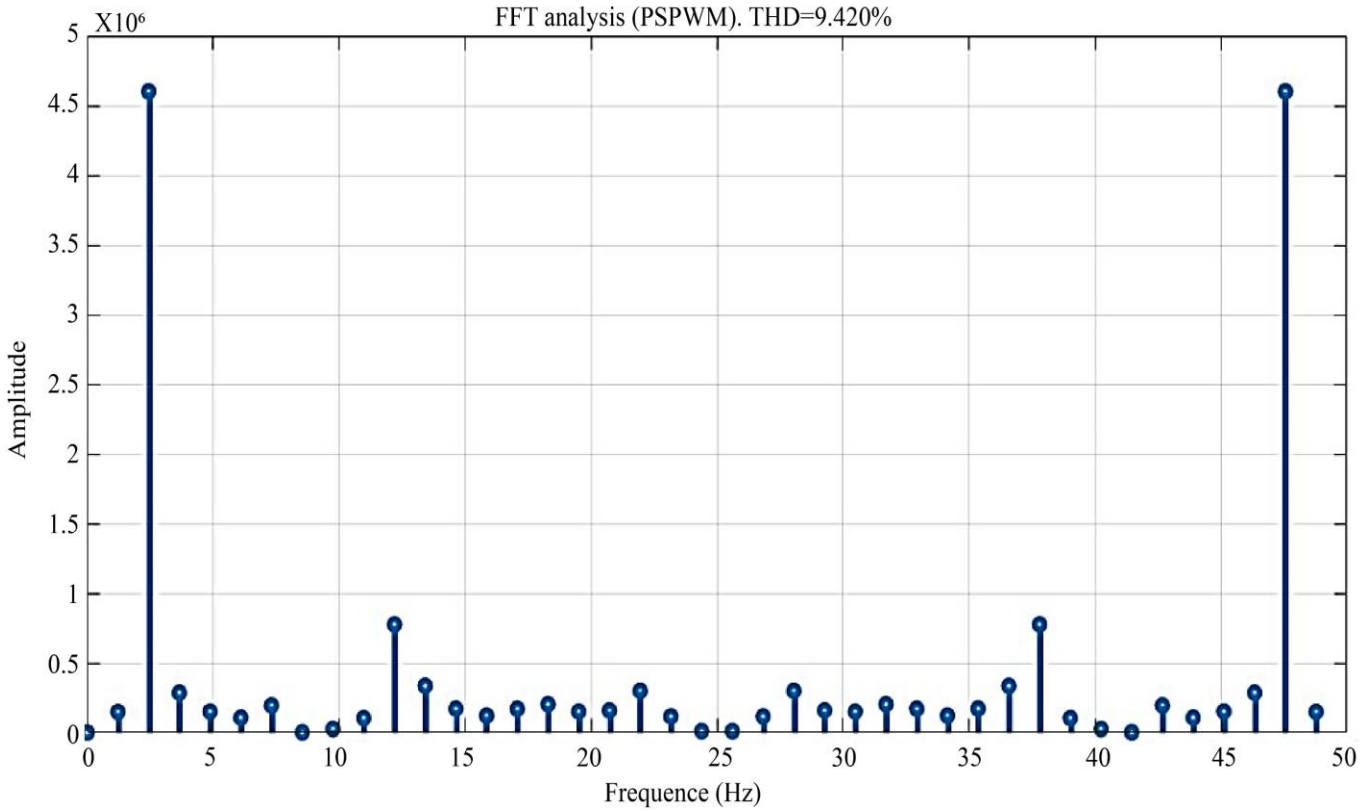

Fig. 16 Evolution of THD for a five-level MMC model with PS-PWM

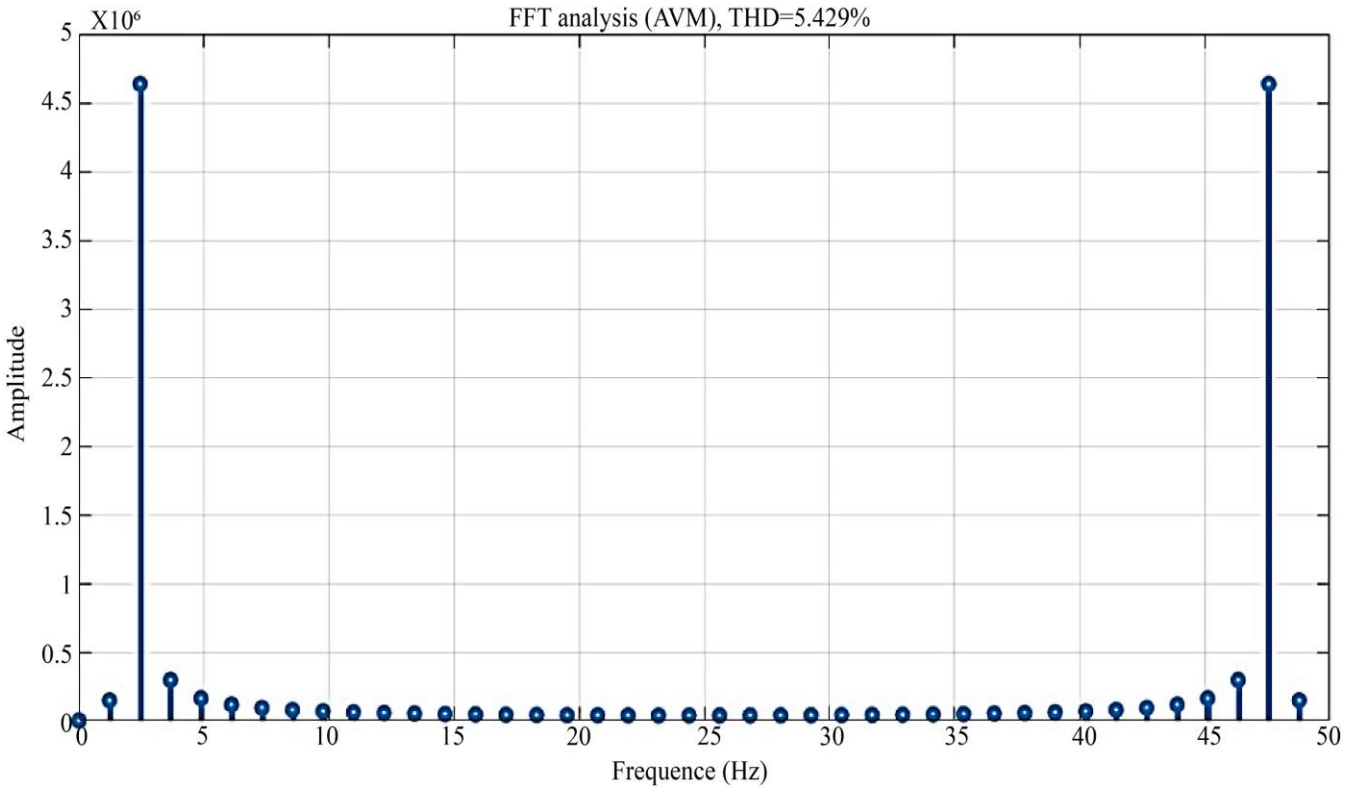

Fig. 17 Evolution of the THD for a five-level AVM-MMC model

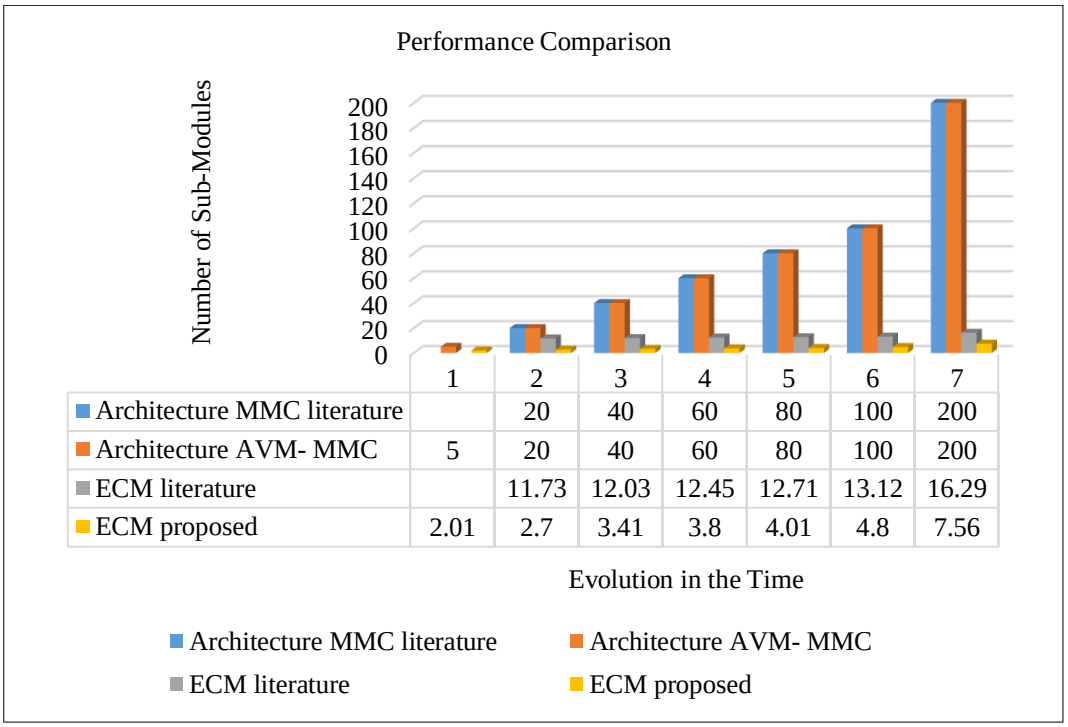

Fig. 18 ECM convergence speed as a function of the number of modules and reaction time

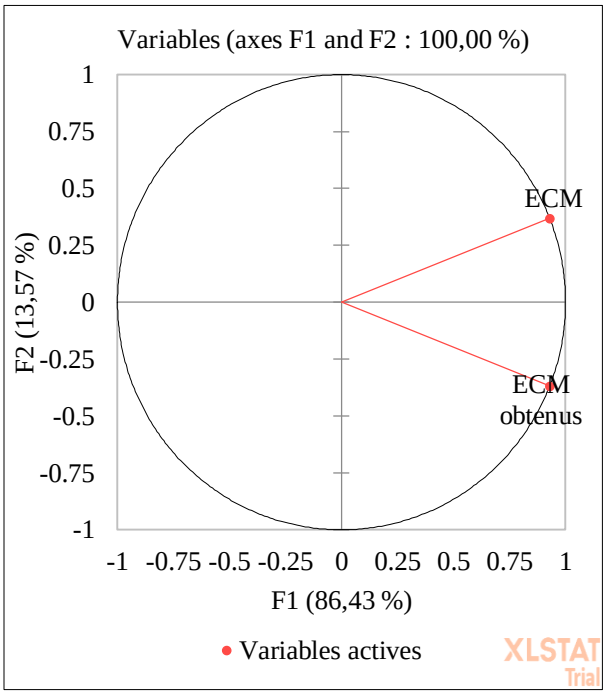

Fig. 19 ECM correlation circle

Table 6. Statistical progression values for seven specific cases

Variable	Comments	Obs. without Missing Data	Minimum	Maximum	Average	Type Deviation
ECM Proposed	7	7	2,010	7,560	4,040	1,796
ECM	7	7	0,000	16,290	11,190	5,161

Figures 16 and 17 compare the THD levels for 5 stages of the two architectures, highlighting the big difference obtained with Figure 17 AVM-MMC model, which gives 5.429% against 9.4% with Figure 16 of the model MMC architecture with PS-PWM. Table 6 presents a direct correlation in terms of statistics for seven specific scenarios in terms of sub-modules with a direct comparison to the literature; the trends in ECM are better in this article. Evidence that numerical modeling improves system performance over time. Figure 19 provides a correlation circle between the ECM obtained and the ECM available in the literature. The F1 component represents the main information for the PCA, which is at 86.43%, and F2 represents the secondary information at 13.57%. The angle between ECM obtained and ECM from the acute literature indicates a positive correlation, highlighting a clear performance.

4. Conclusion

This article aimed to propose an innovative digital modeling of an AVM-MMC architecture for HVDC connection systems and compare its results to a real MMC model under the same operating conditions. Compared to the above, the AVM-MMC architecture offers better execution time by simplifying the computational load due to power switches. It also offers a better THD of 4.6% from 5 modules. This architecture will, therefore, make it possible to optimize the control and supervision of HVDC interconnection systems by evaluating their behavior with many non-linear components. While limiting the impact of THD on the system, the main contributions in this work were therefore:

- Innovative digital modeling is achieved by improving the control and, especially, the complexity of HVDC-MMC systems when the number of modules is large at the level of the converter cell.
- A direct limitation of the resonance phenomenon due to non-linear loads in the converters with a considerable reduction in THD
- Limitation of auxiliary blocks for power quality with filters at converter output
- Compared to the current literature, there is a considerable reduction in the computing power required to control IGBT switches, e.g., submodules.
- Statistical validation based on certain indicators with Principal Component Analysis (PCA)

This work is, therefore, positioned as a multi-objective contribution to the control and supervision strategies of HVDC connection systems. In the perspective of this work, validations in case studies will be developed with several scenarios integrating varied topologies of power switches: IGBT, Thyristors, and Diodes, including indicators such as Yield or Conversion Efficiency, THD, power factor, with the ultimate aim of limiting losses during the transmission of electrical energy on HVDC lines; it is also important to emphasize that with technological advances the sectors of industrial robotics, the automobile industry or even aviation use a lot of electrical energy conversion modules with the same logic or principle of application such what to develop in this work, thus opening up multiple sectors of research for sustainable developments.

Acknowledgements

We thank the Laboratory of Modeling Materials and Methods of the National Higher Polytechnics and the Department of Energetics and Thermal Engineering, University Institute of Technology, for providing the necessary facilities and support.

References

[1] Yihua Hu et al., "Design of a Modular, High Step-Up Ratio DC–DC Converter for HVDC Applications Integrating Offshore Wind Power," *IEEE Transactions on Industrial Electronics*, vol. 63, no. 4, pp. 2190-2202, 2016. [CrossRef] [Google Scholar] [Publisher Link]

[2] Yihua Hu et al., "Fault-Tolerant Converter with a Modular Structure for HVDC Power Transmitting Applications," *IEEE Transactions on Industry Applications*, vol. 53, no. 3, pp. 2245-2256, 2017. [CrossRef] [Google Scholar] [Publisher Link].

[3] Nikolas Flourentzou, Vassilios G. Agelidis, and Georgios D. Demetriades, "VSC-Based HVDC Power Transmission Systems: An Overview," *IEEE Transactions on Power Electronics*, vol. 24, no. 3, pp. 592-602, 2009. [CrossRef] [Google Scholar] [Publisher Link]

[4] Laurent Teppoz, "*Control of a VSC-HVDC Type Conversion System, Stability-Disturbance Control*," Theses, Grenoble National Polytechnic Institute, pp. 1-231, 2005. [Google Scholar] [Publisher Link]

[5] Maryam Saeedifard, and Reza Iravani, "Dynamic Performance of a Modular Multilevel Back-to-Back HVDC System," *IEEE Transactions on Power Delivery*, vol. 25, no. 4, pp. 2903-2912, 2010. [CrossRef] [Google Scholar] [Publisher Link]

[6] Entsoe, "*HVDC Links in System Operations*," Technical Paper, pp. 1-81, 2019. [Publisher Link]

[7] Abdulrahman Alassi et al., "HVDC Transmission: Technology Review, Market Trends and Future Outlook," *Renewable and Sustainable Energy Reviews*, vol. 112, pp. 530-554, 2019. [CrossRef] [Google Scholar] [Publisher Link]

[8] Elisabeth N. Abildgaard, and Marta Molinas, "Modelling and Control of the Modular Multilevel Converter (MMC)," *Energy Procedia*, vol. 20, pp. 227-236, 2012. [CrossRef] [Google Scholar] [Publisher Link]

[9] Martin Funck, and Joseph Vandendorpe, "*HVDC Connections: Structure, Control and Modeling*," VSC and MMC Technologies, Catholic University of Louvain, pp. 1-129, 2016. [Google Scholar] [Publisher Link]

[10] Sébastien Dennetière, "*Contributions to the Modeling and Validation of VSC-MMC type HVDC Link Models in Real-Time Simulation Tools*," Ph.D. Thesis, University of Montreal, pp. 1-24, 2017. [Google Scholar] [Publisher Link]

[11] Hani Aziz Saad, "*Modeling and Simulation of a VSC-MMC Type HVDc Link*," Ph.D Theses, Polytechnic School of Montreal, pp. 1-242, 2015. [Google Scholar] [Publisher Link]

[12] Udana Niranga Gnanarathna, "*Efficient Modeling of Modular Multilevel HVDC Converters (MMC) on Electromagnetic Transient Simulation Programs*," Thesis, University of Manitoba, Winnipeg, pp. 1-224, 2014. [Google Scholar] [Publisher Link]

[13] F. Shewarega, and I. Erlich, "Simplified Modeling of VSC-HVDC in Power System Stability Studies," *IFAC Proceedings Volumes*, vol. 47, no. 3, pp. 9099-9104, 2014. [CrossRef] [Google Scholar] [Publisher Link]

[14] S. Cole, and R. Belmans, "A Proposal for Standard VSC HVDC Dynamic Models in Power System Stability Studies," *Electric Power Systems Research*, vol. 81, no. 4, pp. 967-973, 2011. [CrossRef] [Google Scholar] [Publisher Link]

[15] Do-Hoon Kwon, Young-Jin Kim, and Seung-Ill Moon, "Modeling and Analysis of an LCC HVDC System Using DC Voltage Control to Improve Transient Response and Short-Term Power Transfer Capability," *IEEE Transactions on Power Delivery*, vol. 33, no. 4, pp. 1922-1933, 2018. [CrossRef] [Google Scholar] [Publisher Link]

[16] Fabrice D'eustachio, "*The Challenges of HVDC Systems in Electricity Transmission Networks*," National Conservatory of Arts and Crafts, Associated Regional Center of Grenoble, pp. 1-33, 2013. [Google Scholar] [Publisher Link]

[17] A. Beddard, "Improved Accuracy Average Value Models of Modular Multilevel Converters," *IEEE Transactions on Power Delivery*, vol. 31, no. 5, pp. 2260-2269, 2016. [CrossRef] [Google Scholar] [Publisher Link]

[18] R.F. Mochamad, and R. Preece, "Impact of Model Complexity on Mixed AC/DC Transient Stability Analysis," *13th IET International Conference on AC and DC Power Transmission (ACDC 2017)*, pp. 24-26, 2017. [CrossRef] [Google Scholar] [Publisher Link]

[19] Fangfang Luo et al., "A Circuit-Oriented Average-Value Model of Modular Multilevel Converter Based on Sub-Module Modelling Method," *2017 12th IEEE Conference on Industrial Electronics and Applications*, Siem Reap, Cambodia, pp. 7-12, 2017. [CrossRef] [Google Scholar] [Publisher Link]

[20] M.O. Faruque, Yuyan Zhang, and V. Dinavahi, "Detailed Modeling of CIGRE HVDC Benchmark System Using PSCAD/EMTDC and PSB/SIMULINK," *IEEE Transactions on Power Delivery*, vol. 21, no. 1, pp. 378-387, 2006. [CrossRef] [Google Scholar] [Publisher Link]

[21] Guobing Song et al., "An Improved Averaged Value Model of MMC-HVDC for Power System Faults Simulation," *International Journal of Electrical Power & Energy Systems*, vol. 110, pp. 223-231, 2019. [CrossRef] [Google Scholar] [Publisher Link]

[22] Anton Stepanov et al., "Spurious Power and its Elimination in Modular Multilevel Converter Models," *Electric Power Systems Research*, vol. 190, 2021. [CrossRef] [Google Scholar] [Publisher Link]

[23] Lei Zhang et al., "Improved Equivalent Circuit Model of MMC and Influence Analysis of Simulation Time Step," *IET Power Electronics*, vol. 13, no. 11, pp. 2212-2221, 2020. [CrossRef] [Google Scholar] [Publisher Link]

[24] Jaime Peralta et al., "Detailed and Averaged Models for a 401-Level MMC–HVDC System," *IEEE Transactions on Power Delivery*, vol. 27, no. 3, pp. 1501-1508, 2012. [CrossRef] [Google Scholar] [Publisher Link]

[25] Dohoon Kwon et al., "Modeling of HVDC System to Improve Estimation of Transient DC Current and Voltages for AC Line-to-Ground Fault—An Actual Case Study in Korea," *Energies*, vol. 10, no. 10, pp. 1-18, 2017. [CrossRef] [Google Scholar] [Publisher Link]